

# The Use of Multidimensional Franck–Condon Simulations to Assess Model Chemistries: A Case Study on Phenol

Igor Pugliesi<sup>†</sup> and Klaus Müller-Dethlefs<sup>\*</sup>

York Centre of Laser Spectroscopy (YCLS), Department of Chemistry, The University of York, Heslington, York YO10 5DD, U.K.

Received: August 15, 2005

Multidimensional Franck–Condon simulations of the dispersed fluorescence spectra of phenol generated with geometries obtained from the highly correlated post-Hartree–Fock methods CASSCF, MRCI, and SACCI are presented. While the simulations based on CASSCF and MRCI optimized geometries are very similar to each other and fail to reproduce the experimentally measured intensities faithfully, the simulations obtained from SACCI optimized geometries are very close to the experimental spectra. The code developed for the multidimensional Franck–Condon simulations is described. It is shown that the integral storage problem common to the evaluation of multidimensional Franck–Condon integrals can be overcome by saving all quantities needed to disk. This strategy allows the code to run on computers with limited resources and is very well suited for application to molecules with a very large number of vibrational modes.

## 1. Introduction

Multidimensional Franck–Condon integrals are important quantities in physical chemistry. In spectroscopy, they are directly related to the vibronic transition intensities of polyatomic molecules; in reaction dynamics, they are used to calculate electron transfer rates in chemical and biological processes.<sup>1–4</sup>

A variety of approaches have been developed to evaluate multidimensional Franck–Condon integrals. Among these, the coherent state method of Doktorov et al.<sup>5</sup> has been extensively applied to large polyatomic molecules. Guner et al.<sup>6</sup> was the first to use this method to simulate vibronic spectra of large molecules. Callis et al.<sup>7</sup> applied the method to the fluorescence spectra of indole and Berger et al.<sup>8</sup> to the simulation of vibrational sequence bands of benzene and pyrazine.

Multidimensional Franck–Condon simulations of the dispersed fluorescence spectra of phenol have been carried out by Schumm et al.<sup>9</sup> using  $S_0$  and  $S_1$  equilibrium geometries obtained at the (8,7)-CASSCF/cc-pVDZ level of theory. These simulations reproduced the main spectral features, but the intensities of several vibronic transitions were either under- or over-estimated. A much better agreement between simulation and experiment was obtained by manually altering the  $S_1$  state CASSCF geometry (shortening the C–O bond and elongating along the coordinate of mode 6a) to produce the characteristic quinoidal structure commonly associated with  $S_1$ – $S_0$  electronic transitions. The structural corrections carried out by Schumm et al. have further been corroborated by Spangenberg et al.,<sup>10</sup> who have developed a Franck–Condon fit program that alters the geometries of the states involved in the electronic transition until a best match between the simulated and experimental intensities is obtained. The changes in rotational constants thus produced are indicative of the  $S_1$  structural characteristics mentioned above and provide an excellent comparison to rotational constants determined by ab initio methods, particularly in the evaluation of the inherent weaknesses in excited state methods.

Studies 9 and 10 indicate that vibronic transition intensities are extremely sensitive to the upper and lower state geometries and, therefore, that Franck–Condon simulations of vibronic spectra of polyatomic molecules can provide very accurate means to assess the quality of the calculated ab initio geometries.

Inspired by this fact, in this study, Franck–Condon simulations of the dispersed fluorescence (DF) spectrum of phenol based on  $S_0$  and  $S_1$  equilibrium geometries obtained from CASSCF and the more highly correlated MRCI and SACCI wave functions are presented and compared. A new Franck–Condon program has been developed for this purpose, and like the algorithms in the studies quoted previously, it is based on the coherent state method of Doktorov et al.<sup>5</sup> To provide the reader with a description of the problem and how it was solved computationally, we give a comprehensive account of the underlying theory in section 2, with a description of the computational code in the Appendix of this paper. An in-depth analysis of the ab initio geometries and frequencies can be found in section 3, which also contains a set of rotational simulations of the  $S_1$  origin band. The rotational simulations were carried out using the asymmetric rotor program developed by M. S. Ford.<sup>11</sup> Finally, in section 4, the Franck–Condon simulations of the DF spectra are presented and discussed.

## 2. Theory

The intensity  $I_{k\mu}$  of an electric dipole transition between two vibronic states is proportional to the square of the electric transition dipole moment  $M_{k\mu}$  which in the adiabatic approximation can be written as eq 1.

$$M_{k\mu} \approx \langle \chi_{k,\kappa}(Q) | \langle \psi_\kappa(q, Q) | M(q, Q) | \psi_m(q, Q) \rangle | \chi_{m,\mu}(Q) \rangle = \langle \chi_{k,\kappa}(Q) | M_{k,m}(Q) | \chi_{m,\mu}(Q) \rangle \quad (1)$$

Here,  $\langle \psi_\kappa(q, Q) |$  or  $|\psi_m(q, Q)\rangle$  and  $\langle \chi_{k,\kappa}(Q) |$  or  $|\chi_{m,\mu}(Q)\rangle$  denote the final ( $k, \kappa$ ) or initial ( $m, \mu$ ) electronic and vibrational states, respectively;  $M_{k,m}(Q)$  is the electronic transition dipole moment; and  $q$  and  $Q$  are the electronic and nuclear degrees of freedom. The Born–Oppenheimer approximation generally prevents one from finding analytic expressions of  $M_{k,m}(Q)$ . A Taylor expan-

\* Corresponding author. Present address: The Photon Science Institute, Simon Building, The University of Manchester, Manchester M13 9PL, U.K. E-mail: k.muller-dethlefs@manchester.ac.uk. Phone: +44 (0)161 275 1000.

<sup>†</sup> E-mail: igor.pugliesi@gmail.com.

sion of the transition dipole moment about the equilibrium position  $Q_0$  of the initial electronic state is required to find approximate solutions. If only the first term of the series is considered, the Franck–Condon approximation, which neglects the  $Q$  dependence of the electronic transition dipole moment, is obtained and the evaluation of vibronic transition intensities is simplified to the evaluation of the overlap (Franck–Condon) integral between the vibrational states of the electronic transition of interest (eq 2).

$$M_{\kappa\mu} = M_{km}(Q_0)\langle\chi_{k,\kappa}(Q)|\chi_{m,\mu}(Q)\rangle = M_{km}(Q_0)\left\langle\prod_{r=1}^{3N-6}\varphi(Q'_r)\middle|\prod_{r=1}^{3N-6}\varphi(Q''_r)\right\rangle \quad (2)$$

The vibrational wave functions of the initial and final electronic states are written as products of one-dimensional wave functions  $\varphi(Q_r)$ , which are in turn functions of  $3N$  ( $N$  = number of atoms) normal coordinates  $Q'_r$  and  $Q''_r$  of the initial and final electronic states, respectively. The normal coordinates  $Q_r$  are related to the displacement coordinates  $u_i$  of nucleus  $i$  via eq 3.  $l_{\alpha i,r}$  are the elements of a  $[3N] \times [3N - 6]$  orthogonal matrix  $L$  and relate the mass-weighted Cartesian displacement coordinates to the normal coordinates. It is generated from the ab initio Hessian when a normal-mode analysis is carried out.

$$m_i^{1/2}u_i = \sum_{r=1}^{3N} l_{\alpha i,r}Q_r \quad (3)$$

$L$  depends on the atomic masses and, more importantly, the force constants  $k_{ij}$  and thus is specific to the ab initio method and electronic state for which it is calculated. Consequently, the normal coordinates  $Q''_r$  and  $Q'_r$  also differ and this causes the normal modes of one electronic state to be rotated or mixed in the normal-mode basis of the other electronic state, a phenomenon first considered by Duschinsky.<sup>12</sup> It poses a particular problem when solving eq 2 as it prevents the Franck–Condon integrals from being reduced to simple products of one-dimensional integrals, making their evaluation complicated and computer intensive. Duschinsky proposed that the two sets of normal coordinates  $Q''_r$  and  $Q'_r$  are related to each other by the linear transformation shown in eq 4.

$$Q''_r = \sum_k S_{rk}Q'_k + d_r \quad (4)$$

$$S = (L'')^{-1}L' \quad (5)$$

$$d = (L'')^{-1}M^{1/2}(r''_{\text{eq}} - r'_{\text{eq}}) \quad (6)$$

The *Duschinsky matrix*  $S$  is an orthogonal matrix describing the rotation, and the *normal coordinate* displacement vector  $d$  the translation between  $Q''_r$  and  $Q'_r$ .  $S$  and  $d$  are related to the  $L$ -matrices, the atomic masses, and the equilibrium geometries by eqs 5 and 6.  $L$  has the dimensions  $[3N] \times [3N - 6]$ , excluding the three rotations and three translations of the normal-mode analysis;  $M^{1/2}$  is a diagonal  $[3N] \times [3N]$  matrix with each atom's mass repeated three times;  $r''_{\text{eq}}$  and  $r'_{\text{eq}}$  are vectors of the equilibrium geometries of the initial and final states, respectively.  $S$  can be viewed as an overlap matrix between the normal modes of the two electronic states. The closer the diagonal elements are to unity, the more the normal modes are similar to each other in form and energy. Large off-diagonal elements indicate a change in the energy ordering or mixing between different normal modes. This mixing is the mathematical expression of a Duschinsky rotation.

For the evaluation of  $S$  and  $d$ , it is crucial that the equilibrium geometries are oriented so that the Eckart conditions<sup>13</sup> are fulfilled<sup>14,15</sup> for both states simultaneously. This is generally the case when the atomic coordinates are in standard orientation, the same orientation in which the normal mode analysis is conventionally performed. There are, however, cases where the standard orientation of the two electronic states to be overlapped is largely different and axis switching effects need to be taken into account requiring a more general transformation than the one in eq 4. This problem has been discussed extensively in the literature.<sup>15–17</sup>

Sharp and Rosenstock<sup>18</sup> were the first to solve the Franck–Condon integral problem for polyatomic molecules including the Duschinsky effect. Their equations express individual Franck–Condon integrals by a finite series expansion. This approach was the first of its kind and provided a general basis for later methodologies, one of which is the coherent state method developed by Doktorov et al.,<sup>5</sup> which yields the same expression as the method of Sharp and Rosenstock. The solution of a multidimensional Franck–Condon integral is now achieved by recurrence relations, which are exact in the harmonic approximation. The derivation of these relations can be found in a recent publication by Berger et al.,<sup>8</sup> and thus, only a qualitative explanation of the principles behind it is given here. In short, an analysis of the action of the Duschinsky transformation on the vibrational Hamiltonian expressed in terms of annihilation and creation operators reveals the existence of an operator (which is an element of the Lie group  $\text{Sp}(2N, R) \wedge \text{H}(N)$ , a dynamical symmetry group of the vibrational Hamiltonian) that connects the initial and final Hamiltonians and whose matrix elements are the Franck–Condon integrals. Taking advantage of the fact that coherent states can serve as generating functions for the stationary states (used in eqs 1 and 2) of the vibrational Hamiltonian and that furthermore they are a basis of the dynamical group representation, the overlap integral between the coherent states of the initial and final electronic states can be used as a generating function for the Franck–Condon integrals, which leads to the extraction of recurrence relations for their evaluation. These relations are given in eqs 7 and 8, where the former is used to decrement the final and the latter the initial stationary state vector.

$$\begin{aligned} \langle v'_1, \dots, v'_i + 1, \dots, v'_{3N-6} | \bar{v}'' \rangle = & 2 \sum_{k=1}^{3N-6} R_{ik} \left( \frac{v''_k}{v'_i + 1} \right)^{1/2} \langle v'_1, \dots, v'_i, \dots, v'_{3N-6} | v''_1, \dots, v''_k - \\ & 1, \dots, v''_{3N-6} \rangle + \sum_{j=1}^{3N-6} (2Q - 1)_{3n-6}{}_{ij} \left( \frac{v'_j}{v'_i + 1} \right)^{1/2} \langle v'_1, \dots, v'_j - \\ & 1, \dots, v'_{3N-6} | \bar{v}'' \rangle - (R\delta)_i \left( \frac{2}{v'_i + 1} \right) \langle v'_1, \dots, v'_i, \dots, v'_{3N-6} | \bar{v}'' \rangle \end{aligned} \quad (7)$$

$$\begin{aligned} \langle \bar{v}''' | v''_1, \dots, v''_k + 1, \dots, v''_{3N-6} \rangle = & 2 \sum_{i=1}^{3N-6} R_{ik} \left( \frac{v'_k}{v''_k + 1} \right)^{1/2} \langle v'_1, \dots, v'_i - 1, \dots, v'_{3N-6} | v''_1, \dots, v''_k, \dots, \\ & v''_{3N-6} \rangle + \sum_{j=1}^{3N-6} (2P - 1)_{3n-6}{}_{kj} \left( \frac{v'_j}{v''_k + 1} \right)^{1/2} \langle \bar{v}' | v''_1, \dots, v''_j - 1, \dots, \\ & v''_{3N-6} \rangle + [(1_{3N-6} - P)\delta]_k \left( \frac{2}{v''_k + 1} \right) \langle \bar{v}' | v''_1, \dots, v''_k, \dots, v''_{3N-6} \rangle \end{aligned} \quad (8)$$

The  $[3N - 6] \times [3N - 6]$  matrices  $Q$ ,  $P$ ,  $R$ ,  $J$ , and  $\lambda_w$  and the vector  $\delta$  are defined below. The angular frequencies  $\omega$  in  $\lambda_w$  are related to the normal-mode frequencies  $\mathbf{f}$  via eq 11.

$$Q = (1 + J^T J)^{-1}, P = J Q J^T, R = Q J^T \quad (9)$$

$$J = \lambda_{\omega'} S \lambda_{\omega'}^{-1}, \lambda_{\omega'} = \text{diag}(\omega_1^{1/2}, \omega_2^{1/2}, \dots, \omega_{3N-6}^{1/2}), \vec{\delta} = \hbar^{-1/2} \lambda_{\omega'} \vec{d} \quad (10)$$

$$\omega = 2\pi \frac{c}{f} \quad (11)$$

The  $\langle \vec{0}'' | \vec{0}' \rangle$  overlap is the only integral calculated explicitly. It is shown in eq 12.

$$\langle \vec{0}'' | \vec{0}' \rangle = 2^{[(3N-6)/2]} \prod_{j=1}^{3N-6} \left( \frac{\omega_j}{\omega_j'} \right)^{1/4} \det(Q)^{1/2} \exp \left[ -\frac{1}{2} \delta^T (1 - P) \delta \right] \quad (12)$$

### 3. Ab Initio Results

**3.1. Methodologies.** Three ab initio methodologies have been employed to optimize the  $S_0$  and  $S_1$  geometries of phenol. First, (8,7)-CASSCF/cc-pVDZ calculations have been performed using the same active space employed in several CASSCF studies on phenol published previously.<sup>19,20</sup> It consists of seven  $\pi$ -orbitals, six on the aromatic ring and one on the oxygen, as shown in refs 22 and 23. Second, internally contracted MRCI/cc-pVDZ geometry optimizations of the  $S_0$  and  $S_1$  states of phenol have been performed using the state-specific CASSCF wave functions just described as reference. The MRCI wave functions for the  $S_0$  and  $S_1$  states consisted of 3 282 020 uncontracted configuration space functions (CSFs), which were internally contracted to 170 429 configurations. Third, SACCI/cc-pVDZ geometry optimizations have been carried out using all valence orbitals as active space. For calculation efficiency, the (8,7)-CASSCF/cc-pVDZ geometries were used as starting geometries in the optimization. All single excitation operators were included in the linked term of the SACCI calculations. A level two perturbation selection was carried out for the linked double excitation operators. No R2S2-type unlinked operators were included. This led to an excitation space consisting of 40 377 operators for the SAC and 28 210 operators for the SACCI wave function. Operator guess independent geometry convergence was achieved after seven macroiterations for both states. The geometries thus obtained were used for the subsequent simulations. The Dunning cc-pVDZ basis set was used throughout.

MRCI calculations were performed with MOLPRO version 2002.6<sup>21</sup> and SACCI calculations with Gaussian 03<sup>22</sup> on an IBM RS/6000 (4x Power3 375 MHz 64-bit RISC, model 44P270, AIX 5.1L, 4 Gb RAM, 64 Gb scratch) and Linux PC (2x Pentium III 32-bit, Redhat Linux 9.0, 2 Gb RAM, 16 Gb scratch).

**3.2. Geometries: Rotational Constants and Simulations.** Very accurate rotational constants of the  $S_0$  and  $S_1$  states of phenol have been measured by Berden et al.<sup>23</sup> Table 1 lists these constants together with the constants obtained from the CASSCF, MRCI, and SACCI calculations. Inspection of the values indicates that the rotational constants obtained from SACCI calculations are very close to experiment, while those obtained from CASSCF and MRCI calculations are apparently less accurate. However, while the SACCI  $B$  and  $C$  constants are closer to experiment, in the case of the  $A$  constant, CASSCF

**TABLE 1:  $S_0$  and  $S_1$  State Rotational Constants (in MHz) Obtained from the CASSCF, MRCI, and SACCI Equilibrium Geometries of Phenol**

state	rotational constant	CASSCF	MRCI	SACCI	exptl <sup>a</sup>
$S_0$	$A$	5671.1	5683.5	5693.5	5650.5
	$B$	2630.6	2637.3	2614.7	2619.2
	$C$	1797.1	1801.4	1791.8	1789.9
$S_1$	$A$	5451.4	5359.8	5364.5	5313.6
	$B$	2575.4	2600.3	2626.1	2620.5
	$C$	1738.7	1750.9	1763.0	1756.1

<sup>a</sup> Experimental results taken from Berden et al.<sup>23</sup>

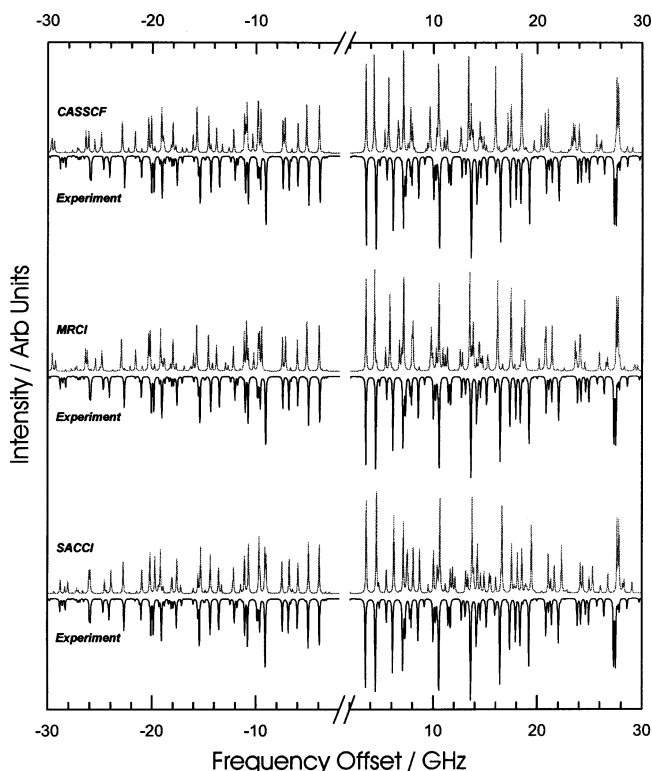


**Figure 1.** High resolution rotational spectra of the  $S_1 0^0$  vibrationless origin. The resolution was set to 75 MHz and the temperature to 1.5 K. To show the quality of simulations compared to experiment, the energy window was reduced to  $\pm 30$  GHz with a break of  $\pm 2$  GHz at the origin (as this region of the spectrum is almost featureless).

delivers a closer value in the ground state and MRCI in the excited state. Thus, inspection alone leaves some ambiguity as to which method has produced the best geometry. To visualize the quality of the calculated geometries, rotational profiles of the vibrationless  $S_1 0^0$  band origin were simulated with the rotational constants in Table 1 and compared to a partially rotationally resolved  $1 + 1'$  REMPI spectrum. The temperature and resolution in the simulations were set to 2.12 K and 1400 MHz, respectively (typical values for the laser experiments conducted at York). The transition dipole moment was set to be essentially parallel to the phenol  $b$  axis (99%  $\mu_b$ , 1%  $\mu_a$ , as per values reported in the literature<sup>19</sup>). The partially rotationally resolved band profiles obtained from the ab initio rotational constants fit the experimental band contour well but look very similar and do not clearly show if any improvements are obtained with the MRCI and SACCI methodologies. To gain a better comparison between theory and experiment, high resolution rotational spectra have been simulated and compared to (a simulation of) the high resolution experimental spectrum of the vibrationless  $S_1 0^0$  origin recorded by Berden et al.<sup>23</sup> In this second set of rotational simulations, the resolution was set to 75 MHz and the temperature to 1.5 K. The high resolution

**TABLE 2: Vibrational Frequencies of Phenol in the  $S_0$  State<sup>a</sup>**

MN	experiment		assignment			(8,7)-CAS NMA on		assignment			(8,7)-CAS NMA on
	B <sup>b</sup>	R <sup>c</sup>	exptl	CASSCF	MRCI	(8,7)-CASSCF geometry <sup>e</sup>	MRCI geometry	SAC			SAC geometry
			R <sup>c</sup>	B <sup>b</sup>	V <sup>d</sup>			R <sup>b</sup>	B <sup>c</sup>	V <sup>d</sup>	
1	244	225	<i>10b</i>	<i>11</i>	<i>10b</i>	249	242	<i>10b</i>	<i>11</i>	<i>10b</i>	244
2	309			$\tau(OH)$		291	306		$\tau(OH)$		381
3	404		15	18b	15	430	429		<i>16a</i>		429
4	409	404		<i>16a</i>		436	431	15	18b	15	430
5	503	504		<i>16b</i>		552	550		<i>16b</i>		545
6	527	526		6a		563	565		6a		563
7	619	618		6b		664	665		6b		662
8	686	686		4		720	720		4		707
9	751		11	<i>10b</i>	11	774	776	11	<i>10b</i>	11	763
10	817			<i>10a</i>		836	838		<i>10a</i>		817
11	823	820	1	12	1	871	878	1	12	1	868
12	881			<i>17b</i>		898	900		<i>17b</i>		882
13	973			<i>17a</i>		975	978		<i>17a</i>		964
14	995			5		1000	1004		5		987
15	1000	999	12	1	12	1068	1073	12	1	12	1073
16	1026			18a		1093	1097		18a		1092
17	1070		18b	15	18b	1144	1151	18b	15	18b	1147
18	1150			9b		1184	1197		9b		1189
19	1169			9a		1251	1256		9a		1253
20	1177	1174		$\beta(OH)$		1271	1276		$\beta(OH)$		1268
21	1343	1349		14		1358	1368		14		1367
22	1262 <sup>f</sup>	1261 <sup>f</sup>	13	7a	13	1382 <sup>f</sup>	1400 <sup>f</sup>	13	7a	13	1383 <sup>f</sup>
23	1277			3		1463	1466		3		1465
24	1472			19b		1597	1603		19b		1600
24	1502	1505		19a		1633	1643		19a		1635
26	1604			8b		1740	1750		8b		1738
27	1610			8a		1758	1773		8a		1768
28	3027		20a	13	7a	3317	3316	20a	13	7a	3355
29	3049		7a	7b	7b	3336	3334	7a	7b	7b	3371
30	3063		7b	2	20b	3348	3346	7b	2	20b	3381
31	3070		20b	20b	2	3361	3360	2	20a	20a	3401
32	3087		2	20a	20a	3370	3369	20b	20b	2	3414
33	3656			$\sigma(OH)$		4162	4158		$\sigma(OH)$		4111

<sup>a</sup> All values are given in  $\text{cm}^{-1}$ . Out-of-plane vibrations are in italics. MN, mode number; NMA, normal-mode analysis; B, assignment by Bist; R, assignment by Roth; V, assignment by Varsányi. <sup>b</sup> Data from ref 24. IR spectra. <sup>c</sup> Data from ref 26. DF spectra. <sup>d</sup> Reference 25. <sup>e</sup> Reference 27. <sup>f</sup> Sometimes called  $\sigma(\text{CO})$  or  $\nu(\text{CO})$ .

experimental spectrum recorded by Berden et al. was reproduced by simulation using the experimental rotational constants reported in ref 23 and listed in Table 1. Figure 1 shows the obtained results. The simulations generated from the SACCI geometries give the best fit to the experiment, with line intensities and energies that are faithfully reproduced in both the P and R branches over a range extending more than 30 000 MHz on either side of the origin. The rotational analysis thus conclusively shows that the geometries predicted by SACCI are of suitably high quality and suggest that improved Franck–Condon simulations will be obtained from these geometries.

**3.3. Normal-Mode Analysis.** The  $S_0$  and  $S_1$  state normal-mode analysis was carried out at the (8,7)-CASSCF/cc-pVDZ level of theory for all three sets of geometries. This strategy was mainly enforced by computation time restrictions, as SACCI and MRCI frequencies on a small molecule like phenol would take unfeasibly long computation times. Performing normal-mode analyses using frequencies obtained at lower levels of theory on geometries obtained from a higher level of theory is generally accepted if the obtained frequencies are comparable to experimental data. This indicates that the frequencies have already been calculated at a high enough level of theory that the benefit of further, higher level, calculations would be at best marginal. In the case of phenol, no negative frequencies were obtained, as the differences between the CASSCF and MRCI/SACCI geometries lay between 0.1 and 1.0 pm and thus are very small. Furthermore, the normal-mode frequencies compare

well to the experimental frequencies of the DF spectra, thus giving some justification for the strategy employed.

As the  $S_0$  and  $S_1$  geometric minima at the SACCI and MRCI levels of theory are displaced with respect to the CASSCF minima, the CASSCF normal-mode analyses on the MRCI and SACCI geometries have large translations, which are, however, within an acceptable limit of  $80 \text{ cm}^{-1}$ . This, and the absence of negative frequencies, suggests that the potential energy surfaces of CASSCF, MRCI, and SACCI are to a first approximation very similar to each other and of reasonably high quality, further justifying the use of CASSCF normal modes and frequencies for the Franck–Condon simulations with MRCI and SACCI equilibrium geometries.

Tables 2 and 3 list the results of the CASSCF normal-mode analyses for the  $S_0$  and  $S_1$  states together with the experimental frequencies and the major schools of mode assignments available in the literature: Bist,<sup>24</sup> Varsányi,<sup>25</sup> and Roth.<sup>26</sup> A schematic representation of the phenol normal modes assigned to the nomenclature of Varsányi can be found in ref 26.

The CASSCF normal frequencies found at the MRCI equilibrium geometries are similar to the frequencies found at the CASSCF equilibrium geometry, with a mean difference of  $4.31 \text{ cm}^{-1}$  in the  $S_0$  state and  $8.47 \text{ cm}^{-1}$  in the  $S_1$  state. The differences between the CASSCF frequencies found at the CASSCF and SACCI equilibrium geometries are much larger, with a mean difference of  $14.72 \text{ cm}^{-1}$  in the  $S_0$  state and  $23.41 \text{ cm}^{-1}$  in the  $S_1$  state. The maximum difference arises

TABLE 3: Vibrational Frequencies of Phenol in the S<sub>1</sub> State<sup>a</sup>

MN	experiment		assignment			(8,7)-CAS NMA on		assignment			(8,7)-CAS NMA on SACCI geometry	
	B <sup>b</sup>	R <sup>c</sup>	exptl R <sup>c</sup>	CASSCF		MRCI	(8,7)-CASSCF geometry <sup>e</sup>	MRCI geometry	SACCI			
				B <sup>b</sup>	V <sup>d</sup>				R <sup>b</sup>	B <sup>b</sup>		V <sup>d</sup>
1	206	162	10b	11	10b	182	164	10b	11	10b	144	
2	187			16a		271	259		16a		240	
3	635			<i>τ(OH)</i>		284	314		4		349	
4	356	465		4		371	364		<i>τ(OH)</i>		388	
5	396		15	18b	15	417	416	15	18b	15	419	
6	441			16b		472	468		16b		458	
7	615	580	11	10b	11	493	491	11	10b	11	474	
8	475			6a		507	510		6a		511	
9	580	615		10a		540	543		10a		517	
10	523			6b		582	582		17a		564	
11	734	700		17a		593	594		6b		580	
12	700	726		17b		616	619		17b		594	
13	726	734		5		701	711		5		708	
14	783		1	12	1	823	833	1	12	1	834	
15	935		12	1	12	969	983	12	1	12	995	
16	962		18b	15	18b	1014	1026		18a		1039	
17	958			18a		1031	1036	18b	15	18b	1040	
18	975			9a		1216	1222		9a		1221	
19	989			9b		1234	1240		9b		1240	
20	1005			<i>β(OH)</i>		1283	1290		<i>β(OH)</i>		1303	
21	1273		13	7a	13	1373 <sup>f</sup>	1397	13	7a	13	1403	
22	1131			3		1437	1443		3		1448	
23	1478			19b		1510	1520		19b		1530	
24	1498			19a		1546	1559		19a		1563	
24				8b		1675	1693		8b		1708	
26	1566			8a		1700	1720		8a		1732	
27	1180	1572		14		1864	1881		14		1895	
28	3084		20a	13	7a	3344	3342	20a	13	7a	3374	
29	3092		7a	7b	7b	3355	3350	7a	7b	7b	3380	
30			7b	2	20b	3371	3369	7b	2	20b	3407	
31	3136		20b	20b	2	3380	3378	20b	20b	2	3413	
32	3186		2	20a	20a	3392	3391	2	20a	20a	3428	
33	3581			<i>σ(OH)</i>		4158	4147		<i>σ(OH)</i>		4090	

<sup>a</sup> All values are given in cm<sup>-1</sup>. Out-of-plane vibrations are in italics. MN, mode number; NMA, normal-mode analysis; B, assignment by Bist; R, assignment by Roth; V, assignment by Varsányi. <sup>b</sup> Data from ref 24. IR spectra. <sup>c</sup> Data from ref 26. DF spectra. <sup>d</sup> Reference 25. <sup>e</sup> Reference 27. <sup>f</sup> Sometimes called *σ*(CO) or *ν*(CO).

between the frequencies of the OH torsion mode (*τ*OH), with values of 89.67 cm<sup>-1</sup> in the S<sub>0</sub> state and 104.29 cm<sup>-1</sup> in the S<sub>1</sub> state. Furthermore, large differences occur in some in-plane modes. The largest are around 30 cm<sup>-1</sup> for the high energy CH and OH stretching modes in both the S<sub>0</sub> and S<sub>1</sub> states.

The energy ordering and the sign (direction) of the displacement of some normal modes are inverted in the CASSCF normal-mode analysis on the SACCI equilibrium geometries. The sign change, however, does not affect the Franck–Condon simulations, as Doktorov’s recursion relations are based on the harmonic approximation; inherent to the harmonic potential is a sign uncertainty in the change of the equilibrium geometry. Expansion or contraction along a normal coordinate gives the same value for the Franck–Condon integral.

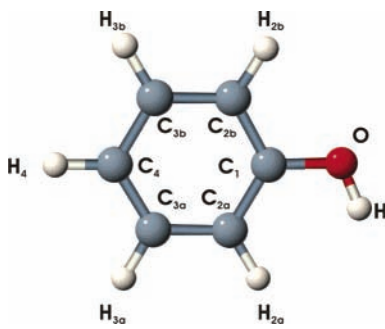
Energy and sign change mainly affect some of the CH stretching and out-of-plane modes, particularly in the S<sub>1</sub> state. This is reflected in a large degree of mode scrambling in the Duschinsky matrix outlined and discussed in the next section. The in-plane modes and the out-of-plane mode 10b seen in the experimental DF spectra are not affected by displacement sign changes and are also very similar in form to the CASSCF normal modes obtained from CASSCF equilibrium geometries. Thus, it can be concluded that the difference in the simulated intensities will be mainly due to differences in the equilibrium geometry, not in the description of the normal modes.

**3.4. Duschinsky Rotations.** It is important to determine if the CASSCF normal-mode analysis on MRCI and SACCI

equilibrium geometries has introduced artificial Duschinsky rotations, which would affect the calculated Franck–Condon intensities and make a comparison of the simulations obtained difficult.

In the following discussion, the mode assignment by Roth based on the Varsányi notation will be used. The plots of the Duschinsky matrices will on the other hand list the modes in terms of ascending energy based mode numbering. To relate this numbering to the assignment by Roth, refer to Tables 2 and 3 for the S<sub>0</sub> and S<sub>1</sub> states, respectively.

The Duschinsky matrix obtained from the CASSCF normal-mode analysis on CASSCF optimized S<sub>0</sub> and S<sub>1</sub> geometries is shown in Figure 2a. As already observed in refs 9 and 10, the matrix can be divided into three blocks of vibrations that do not interact with each other. These include the out-of-plane and in-plane vibrations, which have no interaction with each other, as they belong to different symmetry elements in the G4 symmetry group, and the CH stretching vibrations (20a, 7a, 7b, 20b, and 2) which form a block of their own and do not interact with the other in-plane vibrations. Among the in-plane vibrations, two very strong Duschinsky rotations were observed in ref 9 and are also reproduced in this analysis. The first occurs between modes 12 (or 1 in the notation of Bist et al.<sup>24</sup>) and 18a, and the second, between modes 9b, 14, and *β*(OH). The out-of-plane vibrations show large rotations, which have to be treated with care: the CASSCF active space only contains

TABLE 4: Predicted  $S_0$ – $S_1$  Geometry Changes


	SACCI	MRCI	CASSCF	fit <sup>a</sup>	fit(rot) 1 iso <sup>a</sup>
S <sub>1</sub> –S <sub>0</sub> Bond Length Change/pm					
O–H	0.14	0.08	0.09	0.00	0.00
C <sub>1</sub> –OH	–1.86	–0.97	–0.80	–2.20	–1.90
C <sub>1</sub> –C <sub>2a</sub>	2.83	3.43	3.66	2.30	2.90
C <sub>2a</sub> –C <sub>3a</sub>	2.94	3.30	3.41	2.10	2.40
C <sub>3a</sub> –C <sub>4</sub>	3.00	3.76	4.00	3.30	3.60
C <sub>3b</sub> –C <sub>4</sub>	2.38	3.21	3.43	2.70	2.90
C <sub>2b</sub> –C <sub>3b</sub>	3.14	3.96	4.11	3.00	3.30
C <sub>1</sub> –C <sub>2b</sub>	2.43	2.86	3.04	1.40	2.20
C <sub>2a</sub> –H <sub>2a</sub>	–0.21	–0.24	–0.31	–0.30	–0.30
C <sub>3a</sub> –H <sub>3a</sub>	–0.30	–0.26	–0.26	–0.40	–0.30
C <sub>4</sub> –H <sub>4</sub>	0.28	–0.04	–0.11	–0.20	–0.20
C <sub>3b</sub> –H <sub>3b</sub>	–0.36	–0.28	–0.28	–0.40	–0.30
C <sub>2b</sub> –H <sub>2b</sub>	–0.23	–0.23	–0.14	–0.40	–0.30
S <sub>1</sub> –S <sub>0</sub> Angle Change/deg					
C <sub>1</sub> –O–H	0.29	0.11	0.26	0.10	0.20
C <sub>2a</sub> –C <sub>1</sub> –O	–1.73	–1.34	–1.06	–1.40	–1.40
C <sub>2b</sub> –C <sub>1</sub> –O	–1.46	–0.78	–0.70	–1.00	–1.10
C <sub>1</sub> –C <sub>2a</sub> –C <sub>3a</sub>	–1.87	–1.11	–0.91	–0.60	–0.90
C <sub>1</sub> –C <sub>2b</sub> –C <sub>3b</sub>	–1.46	–0.94	–0.72	–0.40	–0.70
C <sub>2a</sub> –C <sub>3a</sub> –C <sub>4</sub>	–1.32	–0.86	–0.67	–2.30	–2.10
C <sub>2b</sub> –C <sub>3b</sub> –C <sub>4</sub>	–1.43	–1.04	–0.89	–2.60	–2.30
C <sub>2a</sub> –C <sub>1</sub> –C <sub>2b</sub>	3.29	2.12	1.76	2.40	2.60
C <sub>3a</sub> –C <sub>4</sub> –C <sub>3b</sub>	2.99	1.83	1.43	3.60	3.40
C <sub>1</sub> –C <sub>2a</sub> –H <sub>2a</sub>	0.14	0.23	0.30	0.00	–0.20
C <sub>1</sub> –C <sub>2b</sub> –H <sub>2b</sub>	0.19	0.19	0.23	–0.20	0.00

<sup>a</sup> Results taken from ref 10: “fit” marks the geometry changes obtained from the fit to line intensities, while “fit(rot) 1 iso” are the results obtained from a simultaneous fit to line intensities and the experimental rotational constants of *h*<sub>6</sub>-phenol.

$\pi$ -orbitals and thus provides a good description only for in-plane vibrations.

The Duschinsky matrix, obtained from the CASSCF normal modes of the MRCI optimized geometries is essentially identical to the one obtained from the CASSCF geometries and therefore not shown. Conversely, the Duschinsky matrix obtained from the CASSCF normal-mode analysis of the SACCI optimized geometries (Figure 2b) shows some differences. As in the previous matrix, there are three blocks formed by the out-of-plane, in-plane, and CH stretching vibrations. In the in-plane vibration block, the strong rotations between modes 12 and 18a, 9b, 14, and  $\beta$ (OH) are present. However, there are substantial rotations also occurring in the CH stretching block. This is a result of the larger difference between the  $S_0$  and  $S_1$  calculated CH stretching modes mentioned earlier. Thus, a simulation in the CH stretching energy region would have to be treated with care, as the large mode scrambling induced Duschinsky rotations would have a substantial effect on the transition intensities. However, the DF spectra of phenol only show substantial transition intensities in the in-plane vibrations and the out-of-plane vibration 10b, and thus, the artificial Duschinsky rotations in the matrix will not affect the simulation intensities obtained from the SACCI equilibrium geometries. Therefore, the differ-

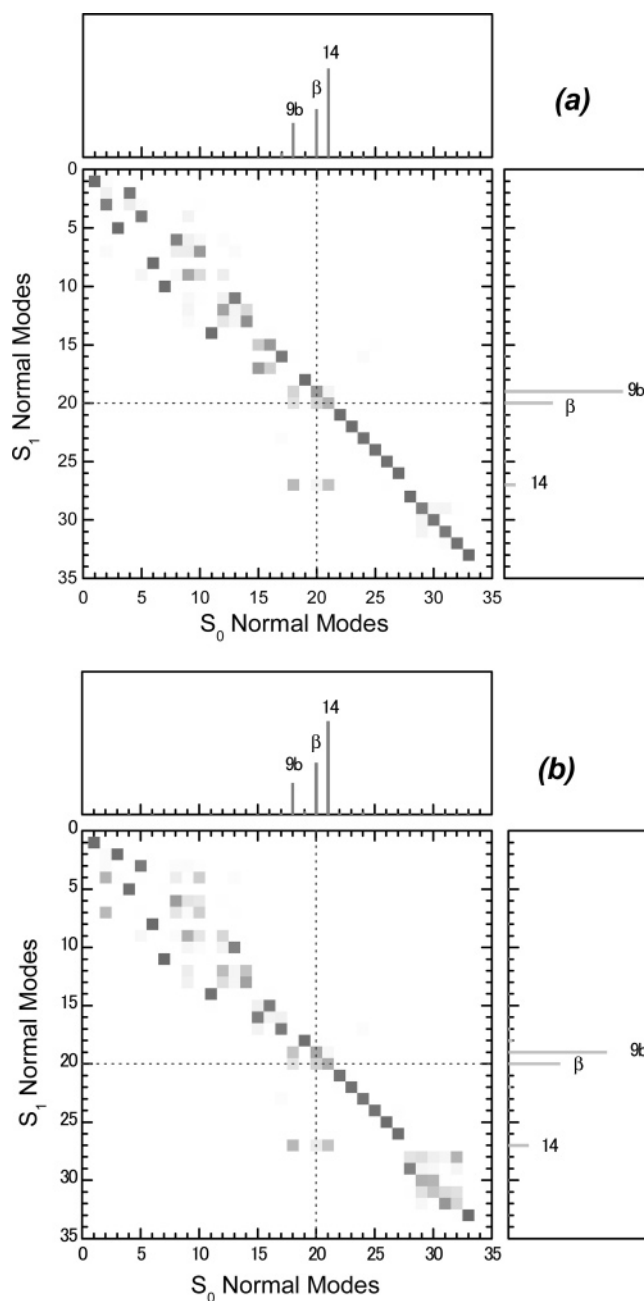


**Figure 2.** Plot of the squares of the elements of the Duschinsky matrix  $\mathbf{S}$  obtained from the CASSCF normal-mode analysis on  $S_0$  and  $S_1$  CASSCF (a) and SACCI (b) geometries. The darker the square, the closer the respective matrix element is to unity. The axes list the normal modes in terms of mode numbers. To relate mode numbering to the assignment by Roth based on the Varsányi notation used in the profile graphs and text, see Tables 2 and 3. The profile graphs show the Duschinsky rotation of mode  $\beta$ (OH) for an  $S_0$ – $S_1$  transition (right profile window) and an  $S_1$ – $S_0$  transition (top profile window). The degree of mode scrambling may be seen by the intensity of off-diagonal components.

ence in intensities will mainly be due to the difference in the  $S_0$ – $S_1$  geometry changes determined at different levels of theory.

#### 4. Franck–Condon Simulations

**4.1. Dispersed Fluorescence Spectra of the Electronic Origin.** Figure 3 shows the experimental and simulated DF spectra obtained from the  $S_1$  electronic origin. As already pointed out in refs 9 and 10, there are substantial differences

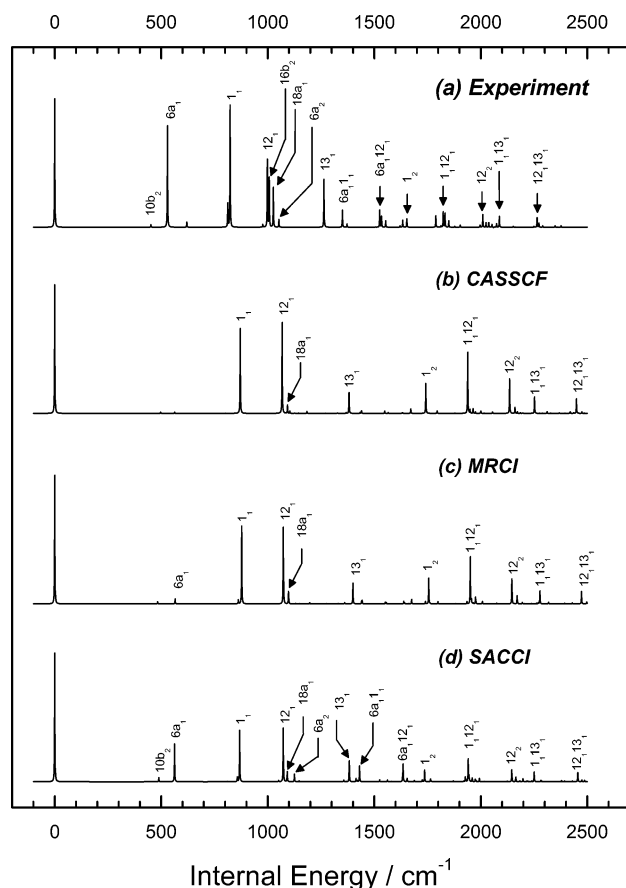


**Figure 3.** Experimental (a) and simulated DF spectra of the electronic origin using (b) CASSCF, (c) MRCI, and (d) SACCI geometries. The largest transition intensities have been labeled following the nomenclature of Varsányi.<sup>25</sup> The intensities are plotted with their associated frequencies listed in Table 2. The experimental spectrum was reproduced by fitting Lorentzian line shapes to intensities taken from ref 10. The subscript number behind a mode indicates the number of quanta in that mode.

between the experimental and simulated DF spectra obtained from CASSCF geometries. Specifically, transitions involving mode 6a are missing from the CASSCF simulation and the simulated intensities of transitions involving mode 12 are too intense. There is only a slight improvement in the intensities obtained from the MRCI geometries. Mode 6a has become slightly more intense, and mode 12 and its combination bands have lost some intensity. On the whole, the spectrum is very similar to the one obtained from the CASSCF geometries. The spectrum obtained from the SACCI geometries shows a very good resemblance to the experimental and fitted spectra of ref 10. Mode 6a and its combination bands now have an appropriate intensity, while transitions involving mode 12 have become considerably less intense.

In the experimental DF spectrum, there is also a very intense band assigned to mode 16b<sub>2</sub> between modes 12 and 18a. This mode is missing in all simulations, the reason for which is a Fermi resonance between modes 12 and 16b<sub>2</sub>. As the method used for calculating Franck–Condon integrals is based on the harmonic approximation, anharmonic effects such as Fermi resonances are not taken into account.

**4.2. DF Spectra of the  $0_0^0 + 10b^2$  Vibronic Transition.** Figure 4 shows the experimental and simulated DF spectra obtained from the vibronic transition  $0_0^0 + 10b^2$ . As with the origin spectrum, mode 12 and its combination bands lose intensity when going from CASSCF and MRCI to SACCI geometries and approach the experimental spectrum in appear-

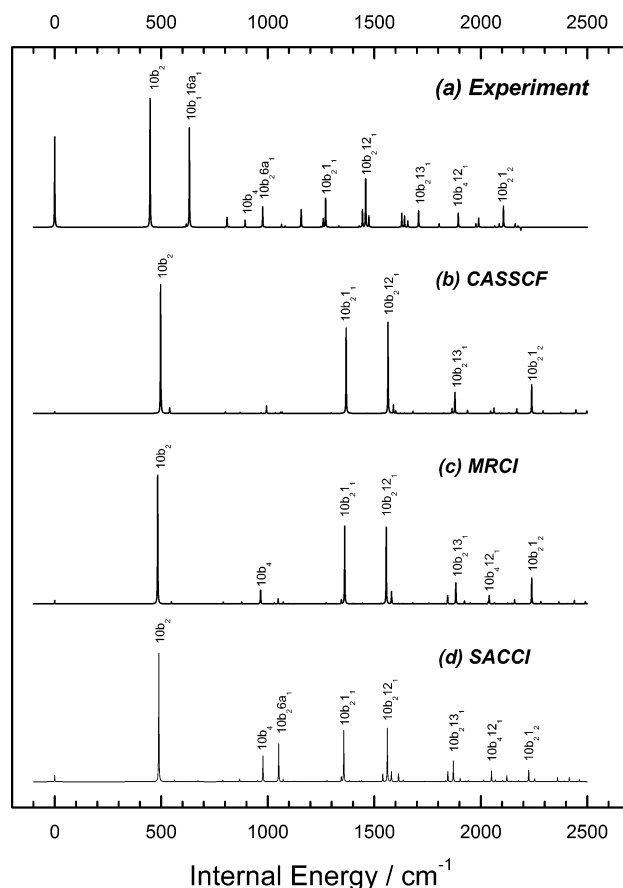


**Figure 4.** Experimental (a) and simulated DF spectra of the  $0_0^0 + 10b^2$  transition using (b) CASSCF, (c) MRCI, and (d) SACCI geometries. The largest transition intensities have been labeled following the nomenclature of Varsányi.<sup>25</sup> The intensities are plotted with their associated frequencies listed in Table 2. The experimental spectrum was reproduced by fitting Lorentzian line shapes to intensities taken from ref 10. The subscript number behind a mode indicates the number of quanta in that mode.

ance. Furthermore, the combination bands involving mode 10b<sub>2</sub> become more intense. In the experimental DF spectrum, there is also a very intense band associated with the 10b<sub>1</sub>16a<sub>1</sub> combination mode, which is missing in all of the simulated spectra. Vibrations 10b and 16a have a'' and a' symmetry (or b<sub>1</sub> and a<sub>2</sub> symmetry in G<sub>4</sub>), respectively, and the combination band therefore has a'' symmetry (or b<sub>2</sub> in G<sub>4</sub>) and is symmetry forbidden. Anharmonic effects, not included in the Franck–Condon treatment, allow this transition to gain intensity, and thus, the band is not reproduced in the simulations.

**4.3. DF Spectra of the  $0_0^0 + 6a$  Vibronic Transition.** Figure 5 shows the experimental and simulated DF spectra obtained from the vibronic transition  $0_0^0 + 6a$ . Band 6a<sub>2</sub> is an intense transition in the DF spectrum but is completely missing in the simulation obtained from the CASSCF geometries. This band acquires some intensity in the MRCI based simulation but gets very intense in the spectrum obtained from the SACCI geometries. Furthermore, the 6a<sub>2</sub> combination bands gain considerable intensity in the SACCI based simulation, duplicating the experiment nicely. Bands 1 and 12 are missing in CASSCF and MRCI but are too intense in the SACCI spectrum, while 6a<sub>1</sub>1<sub>1</sub> and 6a<sub>1</sub>12<sub>1</sub> remain too intense in all simulations.

**4.4. DF Spectra of the  $0_0^0 + 12$  Vibronic Transition.** Figure 6 shows the experimental and simulated DF spectra obtained from the vibronic transition  $0_0^0 + 12$ . The CASSCF based simulation overestimates the intensity associated with band 1. However, in both MRCI and SACCI, the band almost dis-





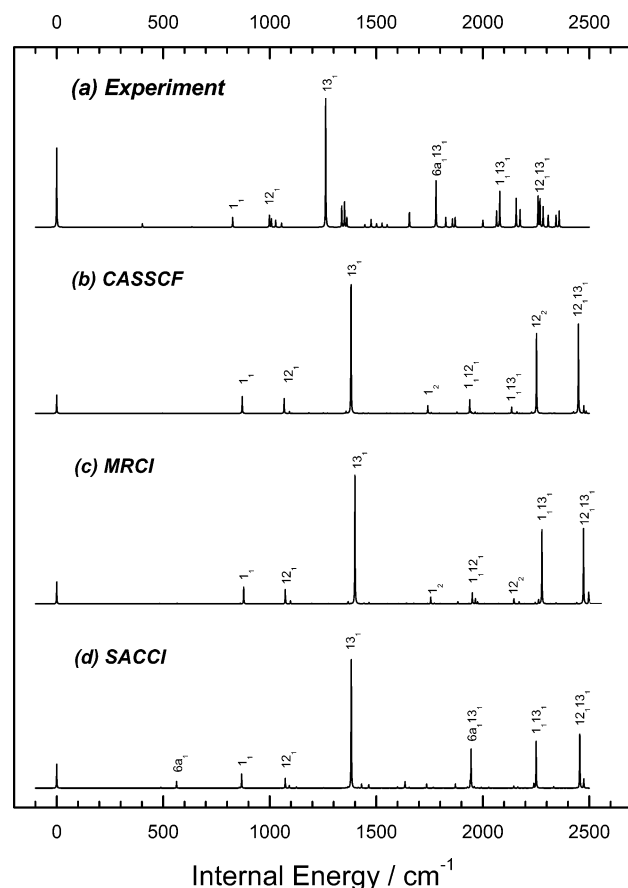


**Figure 7.** Experimental (a) and simulated DF spectra of the  $0_0^0 + \sigma\text{CO}$  (13) transition using (b) CASSCF, (c) MRCI, and (d) SACCI geometries. The largest transition intensities have been labeled following the nomenclature of Varsányi.<sup>25</sup> The intensities are plotted with their associated frequencies listed in Table 2. The experimental spectrum was reproduced by fitting Lorentzian line shapes to intensities taken from ref 10. The subscript number behind a mode indicates the number of quanta in that mode.

of this orbital is 1.99, clearly indicating a small multireference character and thus a minor involvement in the  $S_0$ – $S_1$  bond length change.

One of the major findings from the fits to the DF spectra of phenol in ref 10 was that the quality of the fit is greatly improved by constraining the geometric changes not only to match the experimental vibronic intensities but also to state-specific rotational constants of the molecule, as this avoids overcorrections in the geometries. The fact that the SACCI predicted  $S_0$ – $S_1$  geometry changes are closest to the values obtained from the simultaneous fit to line intensities and rotational constants of six isotopomers of phenol indicates that, in contrast to the geometries obtained from the fit to line intensities only, the SACCI geometries are not overcorrected. However, the predicted SACCI geometry changes suffer from some major shortcomings. Very precise experimental data regarding  $S_0$ – $S_1$  geometry changes have been obtained by Ratzet et al.<sup>28</sup> through fitting of the  $S_1$  state geometry to the inertial parameters of 12 isotopomers obtained from high resolution rotational laser induced fluorescence (LIF) spectra. This group's fits predict a decrease of the C–O bond length similar to SACCI (1.40 pm). However, there is also an increase of the O–H bond length by 1.9 pm; for SACCI, this bond is largely unaffected by the electronic excitation.

The simulations obtained from SACCI geometries suggest that the operator space of the SACCI wave function employed in this study is large enough to yield superior geometries

compared to CASSCF and MRCI, but further improvement would require a bigger operator space spanning a more extended portion of the complete potential energy surface of the molecule.

It is at first sight surprising that only little improvement is gained in the simulations when MRCI geometries are used. The excitation space, from which the MRCI wave function is constructed, is far larger than CASSCF. However, the key ingredient in MRCI is the reference wave function from which the first-order excitation space is generated. The choice of the reference heavily influences the properties that one wishes to describe. In the calculations presented, the CASSCF wavefunction was used as reference. Little improvement is gained compared to CASSCF as the excitations forming the first-order interaction space mainly recover dynamic correlation, which does not play a major role in the description of the quantities needed to obtain good vibronic simulations, specifically the change in the C–O and C–C bond lengths. Thus, further orbitals would have to be included in the reference space in order to obtain a better potential energy surface along modes 6a and 8a. A far larger MRCI wave function would therefore be required to gain some improvement in the simulations, making calculations impracticable even for a small system like phenol.

The SACCI excitation space formed by the linked operators is smaller than the one of MRCI. However, the unlinked terms make it far larger, thus yielding a wave function that is superior to the MRCI wave function based on the (8,7)-CASSCF reference. Furthermore, by virtue of the perturbation selection of the excitation operators, the SACCI wave function contains important excitations, thus giving a much improved performance while still making calculations practicable even for larger systems.

It has been shown that carrying out a CASSCF normal-mode analysis on SACCI optimized geometries, although questionable in terms of its consistency, does not affect the simulated transition intensities and thus offers a cheap alternative strategy for obtaining frequencies on SACCI equilibrium geometries provided that the difference between the SACCI and actual CASSCF equilibrium geometries is not too large. Of course, a more consistent and thorough method would be to carry out the normal-mode analysis at the SACCI level of theory. This would require the inclusion of a large number of operators that span the potential surface along all the  $3N - 6$  normal coordinates. Prior to the normal-mode analysis, a new geometry optimization has to be carried out for this enlarged operator set until operator guess independent convergence is obtained. This method requires very long computation times for phenol and would be impossible to apply to the larger species such as biomolecules.

## 6. Concluding Remarks

This study was a critical test of both the Franck–Condon program developed and used for the simulations presented and various ab initio methodologies that have become available for the calculation of electronically excited states. It forms a basis for calculations and choice of methodologies in the more complicated cases such as clusters and biomolecules. Although the results obtained suggest that the SACCI methodology is the most suitable for generating Franck–Condon simulations that are in good agreement with experimental spectra and should be the only one used for assignments of vibrational bands and vibronic spectra, the possibility that the CASSCF and MRCI methods might perform better in certain cases cannot be excluded. The wave functions recover different parts of the electron correlation, each of which can be more or less important

to the geometric properties and excitation induced geometric changes of the molecule under investigation. Nonetheless, the information gained about the different ab initio methodologies employed using phenol as a test case is very valuable, as one is not completely in the dark about the suitability of various levels of theory in predicting geometries accurately enough to allow easy and accurate distinction between geometric isomers frequently present with biomolecules and clusters through Franck–Condon simulations.

**Acknowledgment.** We thank the EPSRC for funding this work (Grant No. GR/M48451/01). Special thanks go to Dr. M. J. Watkins for the inspiring discussions on electronic structure theory and Dr. M. C. R. Cockett for making useful comments and suggestions in the editing process of this manuscript.

## 7. Appendix

When writing the algorithm used for the Franck–Condon simulations presented in this paper, the aim was to create a code that was capable of running on personal computers without the random access memory (RAM) problems inherent to code developed for this same purpose. This was achieved by using a disk based storage method which still allows for calculations to be performed in a realistic time frame, even on relatively slow processors. Furthermore, filters have been developed to allow direct interface of this program to the Gaussian, MOLPRO, and GAMESS-US computational suites.

The action of the recursion relations in eqs 7 and 8 on a hypothetical overlap integral can be found in the appendices of refs 8 and 9. Those recursion charts clearly show that, in the evaluation process of a single overlap integral, integrals of the same type are needed several times. Thus, efficient execution of the recursion relations 7 and 8 can only be achieved by generating the integrals in a specific order and by storing previously calculated Franck–Condon integrals in the computer memory. This is not an easy programming task, as a simple multidimensional array that uses the set of  $3N - 6$  vibrational quanta as an index would require enormous amounts of random access memory, even when the relations are applied to small molecules. A number of algorithms have been developed to overcome this difficulty, with the most successful approaches being the binary tree algorithm developed by Gruner and Brumer<sup>6</sup> and the three-level-fixed tree algorithm by Ruhoff and Ratner.<sup>29</sup> Schumm et al.<sup>9</sup> implemented a hash table algorithm which has also proved successful.

In the code presented herein, the integrals are written to a dedicated file on the computer hard disk. As the program runs down the recursion branches, it checks if the integral to be calculated has already been written out. The integral is recognized by its associated vibration state vector, which is printed as a string of integers in a standard tab delimited ASCII file. If the integral is found, the program moves up the recursion branches until all loops are closed.

Saving the vibration state vector as a string where there is no white space between the quantum numbers of different vibrations restricts the maximum number of quanta in any one vibration to nine. While this limitation is easily overcome, it was not felt to be a severe restriction, as vibronic progressions with more than six quanta are very rare in vibronic spectra recorded in molecular beams. However, as strings can have up to 256 characters, vectors with a maximum number of 256 modes can be stored, making this method amenable to Franck–Condon simulations of very large molecules.

As the program was written for the simulation of electronic spectra recorded in molecular beams, where the molecules are

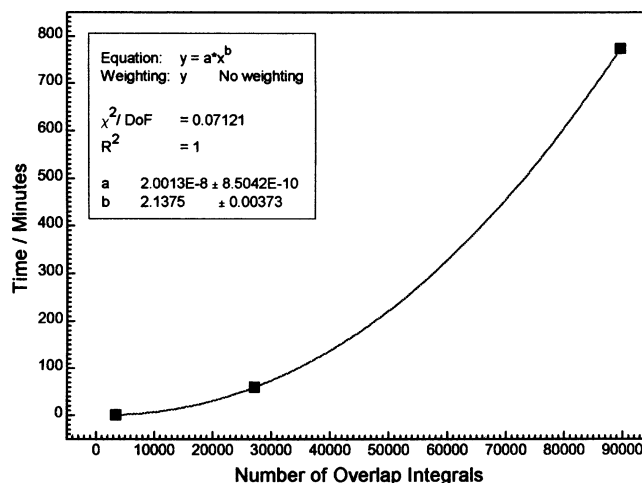


**Figure 8.** Scaling of the computation time with the number of integrals. The inset in the figure shows the results from fitting the function  $y = ax^b$  to the data points.

in the vibrational ground state or a well-defined initial vibronic state which generally does not contain more than two or three vibrational quanta, only integrals of the type  $\langle v_1, \dots, v_{3N-6} | 0 \rangle$ , that is, where the initial state is in the vibrational ground state, are saved, since they constitute the largest number of integrals to be calculated in any one recursion. For the same reason, the program automatically generates all possible quantum combinations in the vibration vector of the final state but lets the user define the quantum state of the initial state vector. To limit the amount of integrals to be calculated, the program checks against a set of user defined restrictions similar to those described in ref 9 as it counts up the quantum numbers in the final state vector. The parameter of major importance is the energy window—equivalent to the spectral range of interest—within which the user wishes to carry out the simulation, as the program only considers vibrations up to the specified maximum energy of this window. Furthermore, the user can restrict the number of modes that can be simultaneously populated in any one vibration vector that is evaluated. The total number of vibrational quanta in all modes and the maximum number of quanta in one mode can also be restricted.

In the Franck–Condon simulations of phenol DF spectra presented in section 5, the energy window was set to be  $2500 \text{ cm}^{-1}$ , the number of simultaneously populated modes to 2, the total number of vibrational quanta in all modes to 20, and the maximum number of quanta in one mode to the already mentioned limit of 9. With the above restrictions, the evaluation of the DF spectrum took 1 min and 32 s on a laptop equipped with an 800 MHz Intel Celeron processor, showing that the storage method implemented can be used for large molecules on small, commercially available computers.

A more extensive set of test calculations geared to analyze the code performance was carried out on a 32-bit PIII machine with a RedHat 9 OS for guanine.<sup>30</sup> In those simulations, the energy window was set to  $2500 \text{ cm}^{-1}$ , which resulted in a vibration string of 37 entries. The maximum number of quanta in each mode was set to nine, and in a set of three calculations, the maximum number of simultaneously populated modes was progressively increased from two, to three, and finally to four. This resulted in the evaluation of 3457, 27 142, and 89 721 overlap integrals, respectively. The times taken by the calculation machine for the respective simulations were 1 min in the first instance, 60 min in the second instance, and 12 h and 53 min in the last instance. These data points are plotted in Figure 8 together with the interpolation line generated from a function

of the type  $y = ax^b$ , where  $y$  is the calculation time and  $x$  is the number of integrals calculated. A fit to the data points results in the parameter  $b$  being close to 2 (fitted as  $2.1375 \pm 0.0037$ ); thus, the program scales with approximately  $O^2$  in the number of overlap integrals  $O$ . The set of data points is certainly small, but the result shown is indicative of the scaling of the code with respect to the change in the number of integrals.

**Note Added after ASAP Publication.** This article was published ASAP on March 21, 2006. Data were corrected in Table 1. The revised version was reposted on March 30, 2006.

## References and Notes

- (1) Sando, G. M.; Spears, K. G.; Kupp, J. T.; Ruhoff, P. T. *J. Phys. Chem. A* **2001**, *105*, 5317.
- (2) Hwang, H.; Rosicky, P. J. *J. Phys. Chem. A* **2004**, *108*, 2607.
- (3) Hwang, H.; Rosicky, P. J. *J. Phys. Chem. B* **2004**, *108*, 6723.
- (4) Borrelli, R.; Peluso, A. *J. Chem. Phys.* **2003**, *119*, 8437.
- (5) Doktorov, E. V.; Malkin, I. A.; Manko, V. I. *J. Mol. Spectrosc.* **1977**, *64*, 302.
- (6) Gruner, D.; Brumer, P. *Chem. Phys. Lett.* **1987**, *138*, 310
- (7) Callis, P. R.; Vivian, J. T.; Slater, L. S. *Chem. Phys. Lett.* **1994**, *244*, 43.
- (8) Berger, R.; Fischer, C.; Klessinger, M. *J. Phys. Chem. A* **1998**, *102*, 7147.
- (9) Schumm, S.; Gerhards, M.; Kleinermanns, K. *J. Phys. Chem. A* **2000**, *104*, 10648.
- (10) Spangenberg, D.; Imhof, P.; Kleinermanns, K. *Phys. Chem. Chem. Phys.* **2003**, *4*, 2404.
- (11) Asymmetric Rotor Simulation (A.R.S.) program written by M. S. Ford, The University of York, 2000.
- (12) Duschinsky, F. *Acta Physicochim. URSS* **1937**, *7*, 441.
- (13) Eckart, C. *Phys. Rev.* **1935**, *41*, 552.
- (14) Hougen, J. T.; Watson, J. K. G. *Can. J. Phys.* **1964**, *43*, 298.
- (15) Sando, G. M.; Spears, K. G. *J. Phys. Chem. A* **2001**, *105*, 5326.
- (16) Hougen, J. *J. Mol. Spectrosc.* **1984**, *114*, 394.
- (17) Lucas, N. J. D. *J. Phys. B* **1973**, *6*, 144.
- (18) Sharp, T. E.; Rosenstock, H. M. *J. Chem. Phys.* **1964**, *41*, 3443.
- (19) Schumm, S.; Gerhards, M.; Roth, W.; Gier, H.; Kleinermanns, K. *Chem. Phys. Lett.* **1996**, *263*, 126.
- (20) Watkins, M. J.; Müller-Dethlefs, K.; Cockett, M. C. R. *Phys. Chem. Chem. Phys.* **2000**, *2*, 5528.
- (21) Amos, R. D.; Bernhardsson, A.; Berning, A.; Celani, P.; Cooper, D. L.; Deegan, M. J. O.; Dobbyn, A. J.; Eckert, F.; Hampel, C.; Hetzer, G.; Knowles, P. J.; Korona, T.; Lindh, R.; Lloyd, A. W.; McNicholas, S. J.; Manby, F. R.; Meyer, W.; Mura, M. E.; Nicklass, A.; Palmieri, P.; Pitzer, R.; Rauhut, G.; Schütz, M.; Schumann, U.; Stoll, H.; Stone, A. J.; Tarroni, R.; Thorsteinsson, T.; Werner, H.-J. *MOLPRO, a package of ab initio programs*, version 2002.6.
- (22) Frisch, M. J.; Trucks, G. W.; Schlegel, H. B.; Scuseria, G. E.; Robb, M. A.; Cheeseman, J. R.; Montgomery, J. A., Jr.; Vreven, T.; Kudin, K. N.; Burant, J. C.; Millam, J. M.; Iyengar, S. S.; Tomasi, J.; Barone, V.; Mennucci, B.; Cossi, M.; Scalmani, G.; Rega, N.; Petersson, G. A.; Nakatsuji, H.; Hada, M.; Ehara, M.; Toyota, K.; Fukuda, R.; Hasegawa, J.; Ishida, M.; Nakajima, T.; Honda, Y.; Kitao, O.; Nakai, H.; Klene, M.; Li, X.; Knox, J. E.; Hratchian, H. P.; Cross, J. B.; Bakken, V.; Adamo, C.; Jaramillo, J.; Gomperts, R.; Stratmann, R. E.; Yazyev, O.; Austin, A. J.; Cammi, R.; Pomelli, C.; Ochterski, J. W.; Ayala, P. Y.; Morokuma, K.; Voth, G. A.; Salvador, P.; Dannenberg, J. J.; Zakrzewski, V. G.; Dapprich, S.; Daniels, A. D.; Strain, M. C.; Farkas, O.; Malick, D. K.; Rabuck, A. D.; Raghavachari, K.; Foresman, J. B.; Ortiz, J. V.; Cui, Q.; Baboul, A. G.; Clifford, S.; Cioslowski, J.; Stefanov, B. B.; Liu, G.; Liashenko, A.; Piskorz, P.; Komaromi, I.; Martin, R. L.; Fox, D. J.; Keith, T.; Al-Laham, M. A.; Peng, C. Y.; Nanayakkara, A.; Challacombe, M.; Gill, P. M. W.; Johnson, B.; Chen, W.; Wong, M. W.; Gonzalez, C.; Pople, J. A. *Gaussian 03*, revision C.01; Gaussian, Inc.: Wallingford, CT, 2004.
- (23) Berden, G.; Meerts, W. L. Schmitt, M.; Kleinermanns, K. *J. Chem. Phys.* **1996**, *104*, 972.
- (24) Bist, H. D.; Brand, J. C. D.; Williams, D. R. *J. Mol. Spectrosc.* **1967**, *24*, 402.
- (25) Varsanyi, G. *Assignments for Vibrational Spectra of 700 Benzene Derivatives*; Wiley: New York, 1974.
- (26) Roth, W.; Imhof, P.; Gerhards, M.; Schumm, S.; Kleinermanns, K. *Chem. Phys.* **2000**, *242*, 247.
- (27) Watkins, M. J. High Resolution Spectroscopy and Ab initio Study of Weakly bound Clusters. Ph.D. Thesis, The University of York, Sept 2000.
- (28) Ratzer, C.; Küpper, J.; Spangenberg, D.; Schmitt, M. *Chem. Phys.* **2002**, *1283*, 43.
- (29) Ruhoff, P. T.; Ratner, M. A. *Int. J. Quantum Chem.* **2000**, *77*, 383.
- (30) Pugliesi, I.; Müller-Dethlefs, K. Manuscript to be submitted for publication.